PERGAMON

International Journal of Multiphase Flow 27 (2001) 1333–1362

International Journal of Multiphase Flow

www.elsevier.com/locate/ijmulflow

Laser-based particle measurements of spherical and nonspherical particles

David Lee Black [a,1], Mardson Q. McQuay [b,*]

[a] *CFD Research Corporation, 215 Wynn Drive, Huntsville, AL 35805, USA*
[b] *Mechanical Engineering Department, Brigham Young University, P.O. Box 24201, 435 CTB, Provo, UT 84602-4201, USA*

Received 29 November 1999; received in revised form 16 January 2001

Abstract

Experiments were performed to collect a detailed set of particle information in a co-axial jet and a swirling flow to assess the influence of particle shape on the particle dynamics. Spherical glass beads and a ground glass powder of the same material and similar size distribution were used for the experiments. The experiments presented also provide a comprehensive data set of particle information in a well-defined laboratory environment suitable for model validation. Results presented were measured with a two-component phase-Doppler particle analyzer (PDPA) and contain detailed particle velocity information for both spherical and nonspherical particles. Significant differences between spherical and nonspherical particles were observed for both co-axial jet and swirling flows in regions where velocity gradients are high. In general, nonspherical particles in the 30–70 μm range were able to follow the gas-phase velocity much better than the spherical particles in the same size range. Size-resolved velocity information was also collected directly below the inlet to measure the different velocity characteristics of different size classes within the overall distribution.

Keywords: Particle; Dispersion; Swirl; Flow; PDPA; Nonspherical

1. Introduction

Multiphase flows are characteristic in many common environments found in engineering applications, where the typical fluid is often a gas containing particles, either solid or liquid. Often these flows can be classified as dilute two-phase flows. Examples of areas where dilute two-phase

* Corresponding author. Tel.: +801-378-4980; fax: +1-801-378-5037.
E-mail addresses: dlb@cfdrc.com (D.L. Black), mq01@byu.edu (M.Q. McQuay).
[1] Tel.: +256-726-4874.

0301-9322/01/$ - see front matter
PII: S0301-9322(01)00008-8

flows are common include pulverized coal combustion, pollutant spread from stack emissions, and the pneumatic transport of powdered material. There has been a continued effort for many years to develop modeling capabilities suitable for predictions of particle dispersion in dilute two-phase flows for use in comprehensive computer codes. The models used to describe the condensed phase are continually being developed and improved. However, complete, accurate experimental information for model evaluation is lacking in the literature (Phillips, 1989; Truelove, 1986; Butler and Webb, 1993). This is especially true for reacting conditions and complex flow structures, such as swirling flows, which are commonly used in many types of industrial burners (Syred and Beér, 1974). To address this need, experiments were performed to collect detailed particle information in a co-axial jet and a swirling flow to assess the influence of particle shape on the particle dynamics and provide a data set suitable for model validation.

Several detailed reviews of the theoretical considerations involved in particle dynamics have been given by past researchers (Bonin, 1992; Shirolkar, 1996; Shirolkar et al., 1996). Included in the review of Shirolkar is a detailed discussion of the theoretical aspects related to particle dispersion and the various methods currently used to model this effect. Other reviews of particle dispersion include those by Lamb (1980), Faeth (1983), and Crowe et al. (1996). These reviews present detailed mathematical descriptions for methods used to model particle dispersion in turbulent flows and describe the relevant physical processes affecting the particles in these flows.

Detailed data useful for model validation for particle predictions in swirling two-phase flows are scarce. One of the most complete studies that has been published so far in this area is the work done by Sommerfeld et al. (1992) and Sommerfeld and Qiu (1991, 1993) using spherical glass beads in an isothermal swirling flow. Although containing comprehensive velocity information at the test condition used in their experiments, only spherical particles were used and no size-resolved data are given. In other related literature, particle velocities in liquid swirling flows for larger spherical particles (510 and 700 μm) were studied by Liu et al. (1989) using an LDV system. They used a fairly high swirl number of 1.38 and reported profiles of mean and RMS velocity.

In addition to work done specifically related to swirling flows, other fundamental particle dispersion studies have been done that provide additional insight on fluid–particle interaction. These research efforts include work done on the effect of particle size distribution on the particle dispersion characteristics (Sommerfeld, 1990), particle dispersion measurements in a turbulent mixing layer (Hishida et al., 1992), and particle measurements in a co-axial jet flow (Call and Kennedy, 1992). Parthasarathy and Faeth (1990) have published results of particle dispersion effects in homogeneous turbulence. They performed experiments on 500, 1000, and 2000 μm particles falling in a stagnant water bath. Good agreement to the standard drag correlations for spherical particles was reported by these researchers, but significant lateral motion of the particles was seen due to particle nonsphericity and eddy-shedding. Modeling turbulent particle dispersion has also been the subject of several recent papers. Wang and Stock (1993) present a detailed discussion of the analysis for the dispersion of a particle in an isotropic, turbulent flow. Frank et al. (1993) describe an analysis for the dispersion of solid particles and include a detailed model of the wall interactions for a two-dimensional channel flow.

An important aspect in particle dispersion studies is the issue of particle shape. The various models used in characterizing the condensed phase rely on the assumption of spherical particles in the development of the mathematical formulation of the model (Shirolkar et al., 1996). However, in actual processes, particles are rarely spherical in nature. Most powders, including pulverized

coal, are manufactured by grinding processesthat produce distinctly nonspherical particles. Since there is potential for particle shape to have a significant effect on the interaction of the solid particle with the fluid (Clift et al., 1978), it is possible for the dispersion characteristics for nonspherical particles to be significantly different than those for spherical particles. Information on the effect of particle shape on the dispersion characteristics is needed to quantify the effect, if any, that particle shape has on the particle velocities and concentrations. No measurements of these types of effects have been found in the literature for realistic flow configurations. However, data of this type are essential in quantifying the error associated with particle dispersion predictions where the assumption is made of spherical particles.

In related areas, a number of researchers have investigated the effect of particle shape on drag. Much of this work consists of determining correlations to predict the drag coefficient for particles of various shapes based on the experimental data available in the literature. Examples include Hartman et al. (1994), Ganser (1993), Haider and Levenspiel (1989) and Swamee and Ojha (1991). All of these researchers show a significant influence of particle shape on the drag coefficient. This is supported by a recent numerical study done by Comer and Kleinstreuer (1995), where they calculated the drag coefficients of nonspherical droplets. They reported that the assumption of spherical particles can result in underprediction of the drag coefficient of up to 30% for some spheroids. The effect of shape on drag and the methods for determining the drag are reviewed by Clift et al. (1978). Since nonspherical particles can have significantly higher drag coefficients, the changes in the interaction of the solid particle with the fluid could be potentially significant.

Although research has been done on the problem of drag for nonspherical particles, no experimental investigations have been undertaken to determine if particle shape has a significant influence on the particle dispersion characteristics in confined flows. The only area related to this issue that has been addressed is the problem of free-falling nonspherical particles in the atmosphere (Klett, 1995). Klett presents a theoretical investigation on predicting the orientation of falling nonspherical particles in the atmosphere. Types of particles considered by Klett include spheroids, disks, cylinders, and ice crystals. That author notes that very small particles tend to be oriented randomly, however larger particles in a turbulent flow field will adopt a preferred orientation with some type of wobbling motion caused by the turbulence. Clift et al. (1978) shows that nonspherical particles in free-fall tend to orient themselves such that the maximum cross-section is in the flow direction. This orientation maximizes the drag forces on the particle and results in the lowest terminal velocity possible for that particular particle. He also notes that for nonspherical particles the drag force is not necessarily parallel to the direction of motion.

The measurements presented here are designed to investigate the differences in the particle velocity caused by particle shape in a confined, nonreacting, swirling and co-axial jet flows. Particles used in the measurements presented here to investigate this effect are spherical glass beads and ground glass powder of the same material and similar size distribution. Measurements were taken on both a co-axial jet and a swirling flow. The co-axial jet flow structure provides a very simple flow environment for looking at variations in particle characteristics without the complications of rapidly changing flow conditions. Swirling flows are widely used in reacting flows for flame stabilization and the data presented provide new information on particle dynamics in this more complex, yet practical, flow structure.

2. Instrumentation

Two types of laser-based particle analyzers were used to collect the data presented here, a two-component, phase-Doppler particle anemometer (PDPA) and a Coulter LS laser diffraction instrument. The PDPA is a nonintrusive, laser-based measurement technique based on measuring the Doppler signal scattered by the particle as it crosses the instrument's sample volume. This method is somewhat insensitive to the amplitude of the scattered light and requires that the particles be spherical. The Coulter LS100 is a diffraction-based system and simply measures the size distribution of the particles without considering velocity or concentration. An extensive review of these instruments, as well as others, has been given by Black et al. (1996).

PDPA instruments have been successfully used for particle measurements in a wide variety of situations for in-situ measurements of particle size and velocity. Breña De La Rosa et al. (1993) used a PDPA system to describe the turbulence properties of a confined swirling spray. Wang et al. (1994a,b) used a similar system for detailed studies of droplet dynamics in a gas turbine combustor. Solid particles have also been measured with the PDPA as shown by studies conducted by Sommerfeld and Qiu (1993). Advantages of the PDPA include better determination of the velocity, the correlation that can be done between velocity and size, and accurate measurements of liquid droplets.

The PDPA instrument used in this study is capable of measuring spherical particles ranging from 0.5 to 650 μm. The size measurement range for a particular instrument configuration and software settings is approximately 50:1. PDPA instruments are single particle counters and have a maximum number density limitation of around 10^6 particles/cm^3. Sizing accuracy under ideal conditions is 4%. The velocities can be resolved from near zero to over 200 m/s with an accuracy of 1% (Bachalo, 1984). In actual measurements these errors increase to some degree, due to errors caused by such factors as the presence of nonspherical particles and variations in the inlet conditions.

The phase-Doppler technique has many advantages, such as providing time-resolved and particle-resolved data, detailed velocity information, and diameter and velocity cross-correlations. However, its use is restricted to spherical particles. This occurs because light scattered by refraction and reflection is used to determine the phase shift in the light scattering signal which is a measure of the local radius of curvature of the particle. Since for nonspherical particles the local radius of curvature can vary by large amounts, the calculated diameter based on the measured curvature can result in large errors in the particle size. Alexander et al. (1985) studied the error associated with sizing nonspherical droplets. They found that the PDPA system overestimated size by 45% for particles with an aspect ratio of 0.71 and underestimated size by 14% for particles with an aspect ratio of 1.39.

Many other studies have also been done in the past to assess the accuracy and reliability of the PDPA instrument (Mcdonell and Samuelsen, 1990; Bachalo et al., 1988; Edwards and Marx, 1992). Imperfection in the optics, beam steering, data collection through optical access windows, changes in temperature, variations in droplet shape, and changes in index of refraction can be sources of potential errors. The PDPA technique has some limitations due to droplet overlapping in dense sprays as discussed in detail by Edwards and Marx (1992). They discussed phase-Doppler measurements in conditions of high number density and determined that the error in measuring droplet number density becomes significant at droplet data-rate levels above 2000–3000 Hz. Mean diameter measurements are not as susceptible to droplet overlapping and can be accurately measured in fairly high-number-density flows.

3. Experimental facilities

A drawing of the experimental facility used for this study is shown in Fig. 1. The cold flow facility (CFF) is designed for a high level of optical access for studies involving nonreacting flows. It is manufactured from a single 183-cm segment of acrylic tube mounted on top of a settling chamber. After the settling chamber there are two additional filters including a cyclone separator and a pleated particle filter prior to the blower. The blower is used to maintain atmospheric pressure inside the flow tube. The most innovative feature of the CFF is the curved windows. The windows are formed from 100-μm thick glass that is taped into place on the inside of a acrylic tube. These windows are thin enough so that they have a minimal impact on the optical systems of laser-based instruments. Curved windows also allow near-wall measurements and eliminate distortion in the flow structure caused by the opening, or flat region, present in the chamber wall when flat windows are used. Five sets of windows (positioned to accommodate the 30° scattering angle of the PDPA) are located along the length of the flow tube.

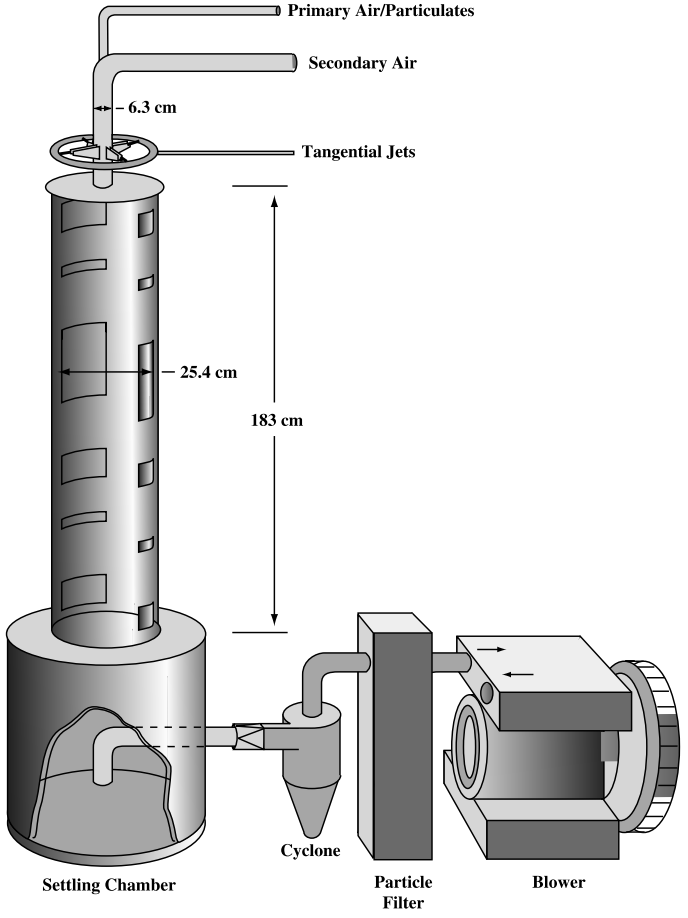

Fig. 1. Sketch showing the design of the CFF.

The facility has a tangential-jet swirled inlet, as shown in Fig. 2. In principle, the inlet is patterned after a similar inlet used for two-phase flow experimentation designed by Hallett (1986). Slight variations on this design are also given by Hallett and Toews (1987) and Hallett and Tavasoli (1991). In this design there is a sliding sleeve that allows the cross-sectional area of the tangential jets to be varied, providing some control over the velocity profile at the exit. For the measurements presented here, these tangential jets were opened 0.3 cm (corresponding to a cross-sectional area of 0.375 cm^2). The secondary air flow passes through two Mitsubishi single-plate flow straighteners manufactured after a design proposed by Akashi et al. (1979). This compact design allows the flow field to reach a uniform velocity profile fairly quickly after passing the 90° bend at the top of the inlet. The primary tube is nonswirled and is designed so that different tubes can be installed on the inlet to have some control over the primary tube diameter. Currently the outer secondary pipe has an inside dimension of 6.27 cm. The inner primary tube has an inside diameter of 0.925 cm and an outer diameter of 1.37 cm.

The facility is mounted on top of a settling chamber to maintain an even velocity distribution across the exit of the tube. The air is pulled from the CFF by the Rotron model 707R blower.

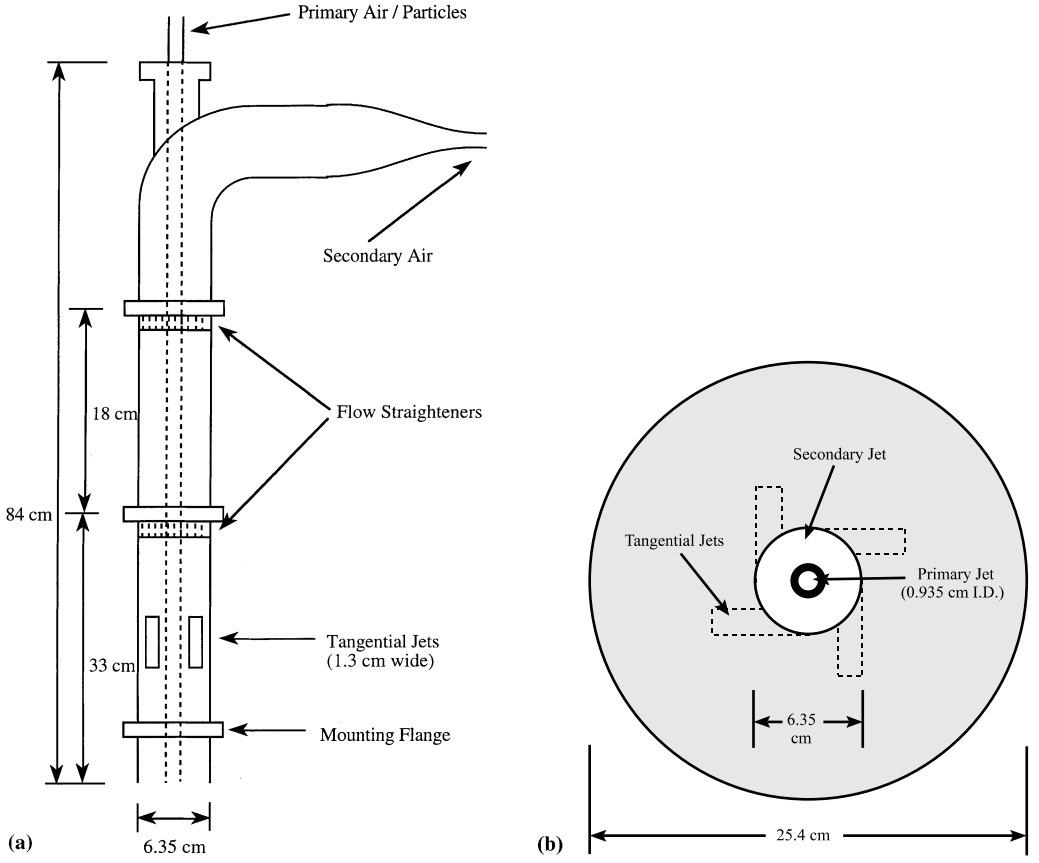

Fig. 2. Diagram of (a) the tangential jet inlet used in the CFF, including (b) a cross-sectional view of the sudden expansion for an observer looking toward the top of the facility.

Airflow is extracted through an inverted 90° elbow to pull air evenly from the settling chamber and avoids distorting the velocity profile at the exit of the tube. The air and particle mixture then passes through a cyclone particle separator and a pleated filter unit to extract all the particles from the flow. The air flow rates in the CFF were measured using three choked-flow orifices. Both the pressure transducers and orifices were calibrated prior to testing to verify correct operation. Accuracy for this type of measuring system is very good, on the order of 2% of the measured flow rates.

Particles used for the experiments consisted of spherical glass beads with a distribution of particles ranging in size from approximately 40–70 μm and a nonspherical glass powder with a similar size distribution. Fig. 3 shows the size distribution of the two powders measured with the Coulter LS100 laser diffraction size analyzer. As shown in this figure, the two distributions have a similar mean; however, the nonspherical particle distribution has a larger spread in the particle sizes. Volume mean diameters were approximately 56 μm for the spherical glass beads and 64 μm for the ground glass powder. The nonspherical particles were prepared by sieving a commercial sand blasting powder between a 230 and 325 mesh screen. This corresponds to 63 and 43 μm. As Fig. 3 shows, the diffraction size analysis shows particles much larger and smaller than the sieve sizes. This is due to the influence of particle shape on the measurements. Fig. 4 shows SEM photographs of the two particle types used in the experiments at the same level of magnification. As illustrated by these photographs, the nonspherical particles are very angular in shape. In addition to the many sharp edges, many of the particles are also very needle-like in structure. The sieve tends to size particles according to the minimum cross-sectional area of the particle; however, diffraction measurements correspond more closely to the volume mean of the particle. For the nonspherical powder used here, the diameter corresponding to the minimum cross-section is much smaller than that corresponding to the average volume of the particles, causing the sieve to undersize the particles.

Both types of particles are fed at a rate of 1 kg/h using an Accurate model 102 volumetric feeder, resulting in a particle loading of approximately 0.01. Spherical particles are fed using a

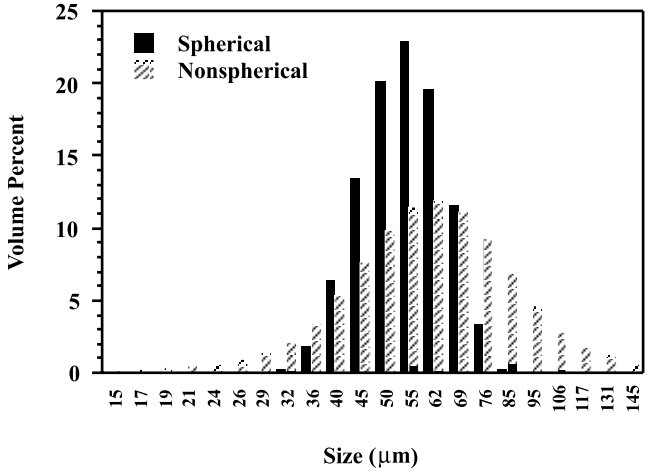

Fig. 3. Particle size distributions for the spherical and nonspherical particles measured with the Coulter LS100.

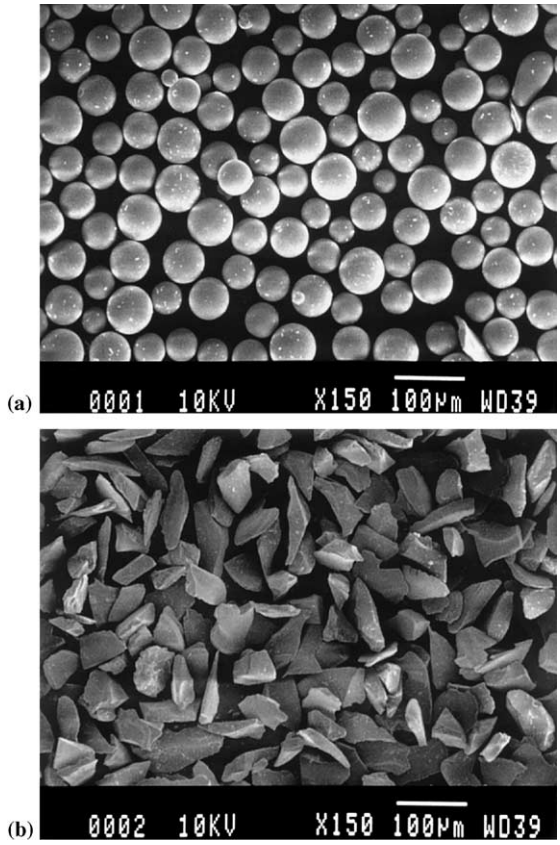

Fig. 4. SEM photographs showing (a) the spherical particles and (b) the nonspherical particles.

hollow core auger with a plate positioned over approximately 3/4 of the end of the feed tube to even out pulsations in the feed rate caused by the rotation of the auger. Due to the angular shape of the particles, the nonspherical glass powder is not as free-flowing as the spherical particles. The nonspherical particles are fed using the same feeder with a solid-core auger assembly, since plugging occurs when hollow-core augers are used. The tube is sealed on the end and has an open notch on the side. The notch is oriented facing upwards and then rotated approximately 45°. This causes the auger to push feed material over the edge of the feed tube, evening out the feed rates. Estimates on the error associated with the particle feed rate is based on repeated measurements at the time of calibration and is approximately 3%.

Particles are entrained into the primary stream with a commercially available eductor. This device uses a high velocity jet of air to create a low pressure region that pulls the particles from the feeder into the primary tube. The amount of air entering the primary stream with the particles is determined by calibrating the system using a wet-test meter. Air to the CFF is supplied by a large tank of compressed air and compressor system at the laboratory. Each flow rate is controlled by a needle valve upstream of the orifice and pressure transducers. Due to the very thin windows used in the facility, the pressure must be kept close to atmospheric pressure to avoid breakage.

Several sets of data were collected during the initial trial measurements in the CFF using the PDPA to verify symmetric and steady operation. To collect velocity profiles very near the location where the particles entered the flow facility, the flow inlet was lowered into the CFF approximately 2.5 cm. This was done to allow measurements to be taken at a location 0.2 cm below the exit plane of the inlet and overcome the constraints on the measurement locations described in the following section. Fig. 5 shows a plot of one initial set of radial profiles for the three components of velocity measured near the exit plane of the inlet. As the data in Fig. 5 show, the flow straighteners and tangential jets worked as designed to produce very symmetric velocity profiles at the exit plane of the inlet. The velocity profiles shown in Fig. 5 correspond to a swirl number of 0.68. Swirl numbers were calculated using a discretized form of the swirl number equations used by Beér and Chigier (1972), neglecting the pressure terms in the swirl number equations.

4. Experimental procedure

The highest location accessible in the CFF in the operating configuration shown for the PDPA is restricted to approximately 1.9 cm below the inlet. This occurs because of the configuration of the receiving optics and the window mounting area needed at the top of the flow tube. At each axial location in the facility where measurements were performed, data were collected from the wall to a location about 4 cm beyond the centerline. In each case, symmetry was very good in the region measured at all axial locations. Due to the symmetric operation of the flow facility, the data shown in this paper are plotted as radial profiles from the centerline of the facility.

Table 1 shows the operating conditions selected for the co-axial jet and the swirling flow test conditions used for measurements of both spherical and nonspherical particles. For all tests, the primary air flow rate and the particle feed rate were held constant at 3 and 1 kg/h, respectively. The air flow rate through the secondary stream was 70 kg/h for the co-axial jet case. For the swirling case, the air flow through the tangential jets was 60 kg/h and the flow through the secondary was 40 kg/h. This set of flow conditions produced a swirl number of about 0.68 at the inlet

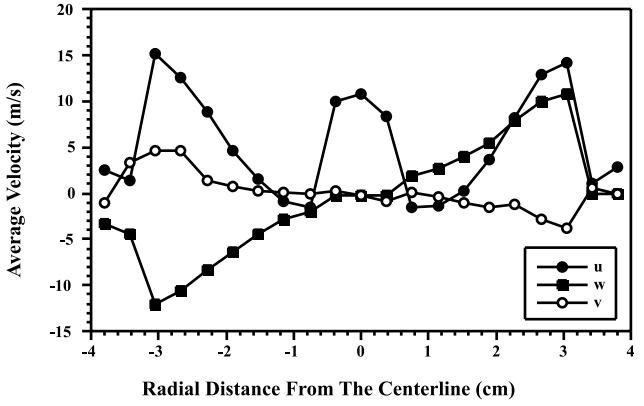

Fig. 5. Velocity profiles 0.25 cm below the inlet at a swirl number of 0.68 showing the high level of symmetry in the flow structure produced by the inlet.

Table 1
Operating conditions and particle characteristics for experiments done in the CFF

Variable	Co-axial jet flow	Swirling flow	Error (%)
CFF operating conditions			
Primary	3 kg/h	3 kg/h	± 3
Secondary	70 kg/h	40 kg/h	± 2
Tangential	0 kg/h	60 kg/h	± 2
Particles	1 kg/h	1 kg/h	± 3
Swirl number	0.0	0.68	
Particle characteristics			
Density	2.46 kg/m^3		
Refractive index	2.45–2.5		

exit. This operating condition was chosen because it produced the highest swirl number that could be measured without having excessive negative velocities near the inlet. The high swirl condition chosen also resulted in a flow structure where the important flow features near the inlet could be easily measured with the top window access. A swirl number of 0.68 is also near the range of those typically found in industrial applications (Syred and Beér, 1974).

Several different procedures in collecting the experimental data were followed depending on the instrument and type of particle being used. Measurements of the gas and spherical particle velocity were done simultaneously using the PDPA by seeding the secondary flow in the reactor with small particles. Nonspherical particles were measured separately using the LDV-only mode of the phase-Doppler instrument. The seeding particles used for these experiments consisted of small glass beads capable of being measured by the PDPA. Seeding particle sizes ranged from approximately 1 to 10 μm, with a mean diameter of approximately 7 μm. This was the smallest spherical particle available that could be sized together with the larger spherical particles using the available instrumentation.

Although not commonly done in the literature, simultaneous measurements of the particle and gas phase velocities using phase-Doppler sizing systems have been done by others, such as Sommerfeld and Qiu (1993) and Mcdonell and Samuelsen (1992). In the data presented here, the gas-phase information is calculated from the measured particles less than 5 μm in diameter. Analysis of the gas-phase velocities along the centerline for the swirling flow case showed that the average and RMS velocities calculated from the particles less than 2 μm in diameter gave the similar results as calculations done using the 5-μm cutoff point. Therefore, the 5-μm level was used throughout the data reduction procedure to maximize the number of particles available for calculating the gas-phase velocity information.

The small seeding particles were entrained into the secondary air stream using a feeding system designed and constructed for the CFF. The feeding system operated by bypassing a portion of the air in the secondary inlet air flow through a tube that terminated near the bottom of a sealed container of seeding particles. Two small holes in the tube caused high velocity jets to stir up the seeding particles in the container. A small amount of seeding particles then exited from the top of the container with the bypassed air and was re-entrained into the secondary air stream.

Histograms measured with the PDPA showed distinctly different results for each particle size class in both the size and velocity information (Black, 1997). Software was written to take the

overall result measured by the PDPA, separate the two distributions, and recompute all the desired parameters for the two particle size classes. The software takes information from the PDPA instrument on particle size, both components of velocity, particle arrival time, and the particle gate time. This information is used to separate the data for each particle class, recalculate all the statistics, and determine the coincident particle information. The coincident criteria used for the data reported here was that the particle had to be in the probe volume formed by both the blue and green beams for a finite amount of time.

5. Results and discussion

Results are presented here for a detailed set of particle data using both spherical and nonspherical particles. Measurements were collected on both a co-axial jet flow and a swirling flow. A co-axial jet flow was first done to capture any differences in the particle dynamics between spherical and nonspherical particles in a simple flow environment. A swirling flow was then investigated, since this type of flow field is widely used in a wide variety of combustion applications. Most of the data were collected near the inlet, since this is the region where velocity gradients are highest. For the co-axial jet case, profiles were measured at the CFF centerline at locations 2.54, 25.4 and 142 cm below the inlet. For the swirling flow case, profiles were taken at these same locations and additional data were collected at a location 10.8 cm below the inlet.

The data collected provide three-dimensional velocity information in the flow facility with both the mean and RMS velocity data. These data provide a detailed set of gas-phase particle data for model validation and highlight the differences in particle dynamics that can occur due to variations in particle shape. Only velocity data, including size-resolved velocity data, in the upper section of the flow facility near the inlet are reported here. This is the region where gradients are high, and where the differences between particle types and the gas phase are the greatest. Additional data beyond those presented here, including additional information on the particle diameters and concentrations can be found in Black (1997).

5.1. Co-axial jet flow

The co-axial jet flow structure is characterized by a central jet of air coming from the inlet into the flow chamber with a sudden expansion to the flow chamber diameter at the exit plane of the inlet. This central jet establishes a weakly recirculating flow that moves upward along the wall, then across the top of the chamber and back toward the central jet of air. In this flow structure, the velocity is nearly one-dimensional, as the tangential velocity component is zero and the radial components are typically small compared to the axial component of velocity.

Measured profiles with each instrument include a vertical profile along the centerline approximately 2 cm below the inlet and radial profiles at locations 2.54, 25.4 and 142 cm below the inlet of the flow facility. The vertical profile along the centerline together with the radial profile done at 2.54 cm below the inlet capture the essential structure of the flow in the region where the gradients are the highest and the flow structure is changing rapidly. Preliminary radial profiles done at a location 10.8 cm below the inlet showed that, for the co-axial jet case, there were no large changes in the flow structure from the information obtained 2.54 cm below the inlet.

Therefore, a radial profile done in the window located 25.4 cm below the inlet was done to characterize the development of the flow field. The measurement location 142 cm below the inlet was the furthest location axially from the inlet where complete radial profiles could be done.

For the co-axial jet flow condition, only the axial component of velocity is reported here as the tangential component was essentially zero over all the measurement locations. However, the RMS velocity in both the axial and tangential directions is presented to characterize the fluctuations. Gas phase and spherical particle size and velocity data were collected simultaneously as discussed in the previous section. Fig. 6 shows the measured axial velocity along the CFF centerline starting 1.9 cm below the inlet. Plotted in the figure are the gas-phase velocity, the spherical particle velocity, and the nonspherical particle velocity. Since no seeding particles are present in the nonspherical particle velocity measurements, the assumption was made that the seeding particles have an insignificant impact on the turbulent flow structure when comparing the information obtained on each particle type. This is reasonable since the seeding particles, and the corresponding loading, are both very small.

In the profiles shown in Fig. 6 the nonspherical particles behave very similar to the gas phase, starting at a peak velocity of around 11 m/s and then decaying to a velocity of about 9 m/s at a location 12 cm below the inlet. However, measurements of the spherical particle velocity first increase over the first 6 cm and then start to decay, reaching a value of 9.4 m/s at a location 12 cm below the inlet. Overall, the nonspherical particles are essentially following the gas phase, while the spherical particles are still accelerating slightly as they enter the flow facility. This information indicates that the nonspherical particles are able to respond faster to the changes in the gas phase as expected due to the higher drag coefficients associated with these particles. The higher drag on nonspherical particles gives them a smaller particle response time. Also, for nonspherical particles, the drag forces are not necessarily in the direction of motion. The dependency of particle orientation on the direction of the forces acting on a particle would cause the nonspherical particles to exhibit a more random behavior in their fluctuating velocities than the spherical particles. This type of effect helps nonspherical particles behave more closely to the turbulent gas phase.

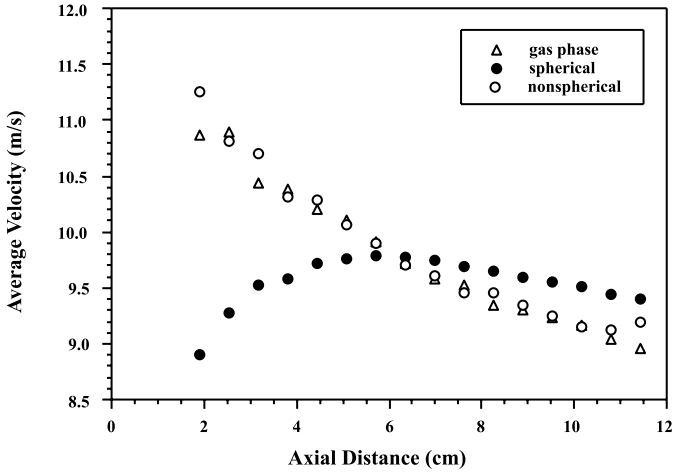

Fig. 6. Axial velocity profiles along the CFF centerline for the co-axial jet case.

Figs. 7(a) and (b) show the RMS velocities measured in the axial and radial directions, respectively, for both particle types and the gas phase. In the axial direction, the two particle types show very similar values of RMS velocity. The RMS velocity for the gas phase in the axial direction (Fig. 7(a)) starts out about 23% greater than the corresponding value for the spherical and nonspherical particles. However, the gas RMS velocity in the axial direction decays somewhat more rapidly than the particle RMS velocities and the measurements for both the gas phase and the two particle types are approaching a common value of approximately 0.8 m/s at the last measurement location (12 cm below the inlet). The RMS values in the radial direction (Fig. 7(b)) show that the spherical particle RMS value initial decays a little more rapidly than the values measured for the nonspherical particles and the gas phase. As in the axial direction, the RMS values for both particle types begin to approach that of the gas phase as they move down from the inlet. Although the nonspherical particles respond faster to the gas-phase velocity fluctua-

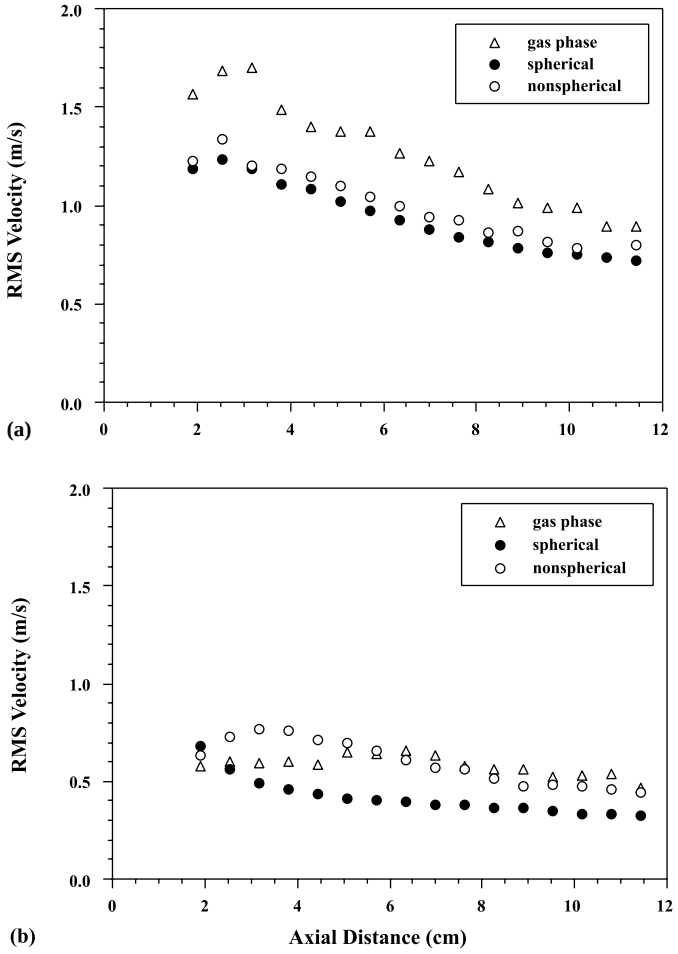

Fig. 7. RMS velocity profiles along the centerline for the co-axial jet case showing (a) the axial component and (b) the radial component.

tions than the spherical particles, they still have a significant amount of inertia. The impact of the particle inertia in regions where the velocities are high, such as those in the axial direction near the inlet, is more evident than in areas where the velocities are low. In the axial direction, the RMS velocity for the nonspherical particles is lower than the gas-phase velocity RMS as shown in Fig. 8(a). This occurs because in areas where the RMS velocity is high, the momentum of the particles tends to decrease the fluctuating velocity component. In the radial RMS component, the mean velocity is essentially zero and the nonspherical particles are then able to respond faster to the gas phase and tend to have the same RMS velocity as the gas phase, as shown in Fig. 8(b).

For the co-axial jet flow, the measured results of axial velocity 2.5 cm below the inlet are shown in Fig. 8 and the corresponding RMS velocities in the axial and tangential directions are shown in Fig. 9. The locations of the wall for the primary air inlet tube and the edge of the tangential jet inlet (as shown in Fig. 2) are indicated in Fig. 8. In regions where velocities were very low, beyond 4 cm from the centerline, there was no detectable difference in the velocities between the particles. The negative velocities measured in this region for the particles and the gas phase are consistent with the weakly recirculating flow established by the co-axial jet. In the high velocity region underneath the inlet, measurements of the nonspherical particles and the gas phase velocities produced very similar results. At the centerline of the flow facility, the gas-phase velocity was about 11.25 m/s, the nonspherical particle velocity was about 10.5 m/s, and the spherical particles were moving at an axial velocity of 9.25 m/s. The secondary and tangential jets are clearly evident in the velocity profile, with the high center peak located directly under the tangential jet followed by a flat profile in the 1–3 cm region under the secondary jet.

The RMS velocity information shown in Fig. 9 shows that the gas phase and the nonspherical particles produce very similar results, except in the axial direction at the centerline. At that location both particle types have axial RMS velocities of about 1.4 m/s. RMS velocity measurements underneath the inlet jets also show a high degree of variability. This is due to the presence of multiple shear layers in the jets caused by the velocity mismatch between the primary jet, the

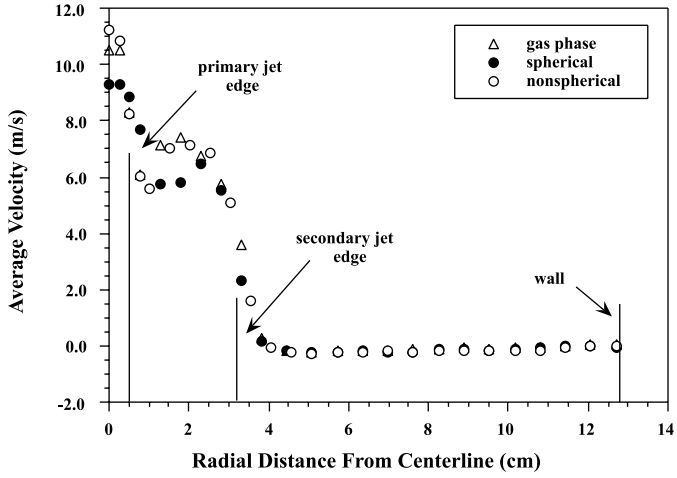

Fig. 8. Radial profiles of axial velocity 2.5 cm below the inlet in a co-axial jet flow.

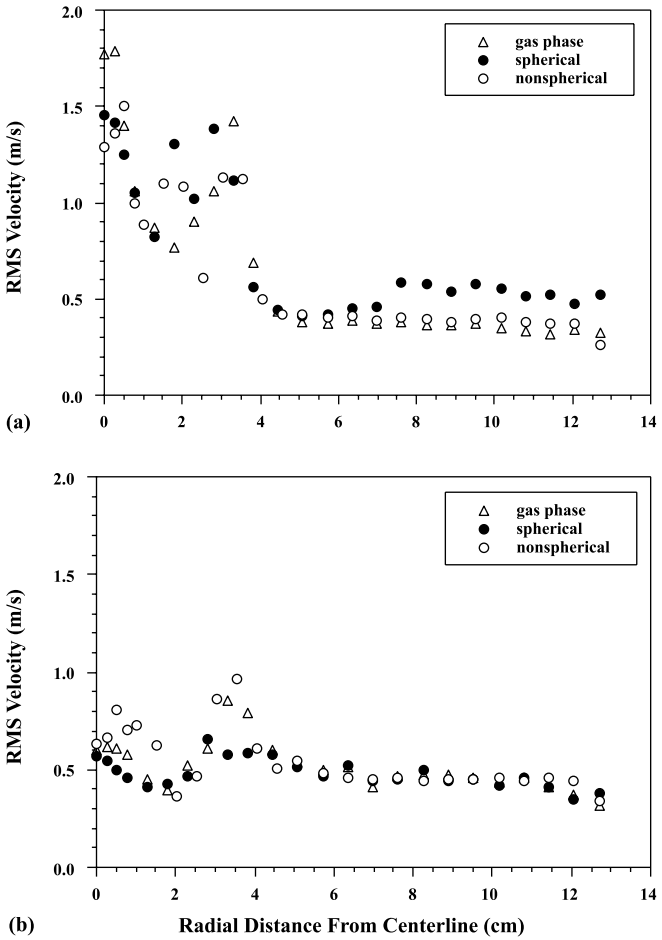

Fig. 9. Radial profiles of RMS velocity 2.5 cm below the inlet in a co-axial jet flow showing (a) the axial and (b) the tangential velocity components.

secondary jet, and the surrounding slowly moving air. The large gradients present in velocity cause a high level of intermittency in the flow field in this region. This results in high RMS velocities with a corresponding high degree of variability.

In addition to the rapidly changing flow structure in this region, the measured particles present can come from one of two places. Particles can either disperse in from the primary jet stream or can be carried in by the recirculating flow field established in the region near the wall. Particles from these sources produce a wide range of particle velocities, as the high velocity particles from the center jet are mixing with the slow moving particles from the recirculating flow. This tends to further increase the RMS velocities in this region. Evidence of the weak recirculation of the flow in the co-axial jet case is shown by the relatively small negative mean axial velocities observed for both particle types and the gas phase beyond the radial location of about 3.5 cm (Fig. 8). From about this location, the tangential RMS velocity component of the gas phase and the two types of particles, shown in Fig. 12(b), show no distinct differences. In the axial direction (Fig. 9(a)), the

RMS velocities in the area closer to the wall for the spherical particles have a slightly higher RMS value than the nonspherical particles and the gas phase. In this region where velocities are moving upward in the flow chamber, the influence of gravity and drag on the particles gives them a greater range of average velocities and therefore a higher RMS velocity.

Velocity measurements at a location 25.4 cm below the inlet showed that the distinctive boundaries between the flow from the primary jet and the secondary jet are gone. The magnitude of the velocity at the centerline also decays in the axial direction to approximately 8 m/s and the jet spreads significantly. At this location, there is little difference between the profiles measured for the two particle types and the gas phase, indicating that the larger particles of both types have reached equilibrium with the gas phase and are essentially able to follow the mean flow path. Since no significant differences were observed, plots of this data are not presented here (see Black, 1997 for the complete data set). The RMS values for the axial component of velocity are also similar for both particle types and the gas phase. RMS velocities start at 0.65 m/s on centerline, increase to 1.7 m/s at a radial location 3 cm from the centerline, decrease to 0.5 m/s at the 7-cm radial location, and then remain nearly constant. The RMS velocity for the tangential component is very similar for the gas phase and nonspherical particles. The measured profile for the spherical particles tends to be flatter than for the other two profiles in the tangential direction, due to the higher response time associated with spherical particles that makes them less sensitive to changes in the turbulent gas-phase motion. In the tangential direction, RMS values are low near the wall and the centerline (0.4 m/s) and peak at a value of 1.0 m/s about 3 cm from the centerline for both the gas phase and the nonspherical particles. Spherical particles follow a similar trend, with RMS velocities starting at 0.35 m/s and peaking at 0.65 m/s. Beyond a radial location 7 cm from the centerline RMS velocities for all particle types are constant at 0.5 m/s. The measured RMS peaks where the gradient in the velocity profile is maximum (at about 3 cm from the centerline), then decreases to the centerline value as the velocity gradient tends toward zero. A similar trend is seen in the profile of the radial component of RMS velocity.

The lowest location where complete profiles can be measured in the facility is located 142 cm below the inlet. At this location in the facility, relatively far from the inlet as compared to the other measurement locations, profiles in both mean and RMS velocity are essentially flat in the radial direction. Also, no significant variations were observed in the axial direction showing that gradients in this direction were insignificant. This indicates that the jet at this location has completely spread out across the diameter of the flow chamber and the flow is essentially a downward moving, turbulent pipe flow. Spherical particles had an average axial velocity of approximately 0.5 m/s while the corresponding value for the nonspherical particles and the gas phase was about 0.35 m/s. In this part of the flow facility, the terminal velocity of the particles can become a significant factor. As previously discussed, nonspherical particles tend to have higher drag coefficients and lower terminal velocities than spherical particles (Haider and Levenspiel, 1989). This effect seems to dominate at the location 142 cm from the inlet resulting in spherical particles having a higher mean velocity than either the gas phase or the nonspherical particles. The RMS values for both axial and tangential components at this location were constant for all particles types in both directions with a value of about 0.3 m/s. A complete discussion and presentation of the data at the 25.4- and 142-cm locations for the co-axial jet flow can be found in Black (1997).

5.2. Swirling flow

Moderate to high swirling flows are characterized by an upper recirculation zone in the corners and a large primary recirculation bubble in the center. The velocity characteristics of these types of flows have been well characterized (Gupta et al., 1984; Syred and Beér, 1974). The recirculating, swirling flow structure produces several stagnation points in the flow that can be used to describe and characterize the flow. The stagnation points of interest include one at the wall separating the flow moving upward along the wall in the upper recirculation zone from that moving down the wall in the lower recirculation bubble. Also there is another significant stagnation point along the centerline near the top where the upward moving flow on the centerline in the lower recirculation zone stagnates against the downward flow from the inlet.

For the swirling flow study, in addition to the profiles measured in the co-axial jet case (i.e., vertical profiles along the centerline near the inlet and radial profiles at the axial locations of 2.54, 25.4, and 142 cm below the inlet), an additional radial profile was measured at 10.8 cm and a vertical profile along the wall in the upper part of the facility was also measured. The additional profiles were done to expand the amount of data in the critical region near the inlet and to locate the stagnation point along the wall corresponding to the boundary between the upper and lower recirculation zones established by the swirling flow field. Again, only limited information is shown in this paper at the upper measurement locations in the flow facility. Complete details are presented by Black (1997).

5.3. Velocity

Measurements of particle velocity in swirling flows are complicated by the strongly three-dimensional structure of the flow field, in contrast to the primarily one-dimensional structure seen in the co-axial jet flow condition. PDPA measurements were done to provide a three-dimensional image of the velocity flow field in the CFF at the chosen operating condition. The position of the

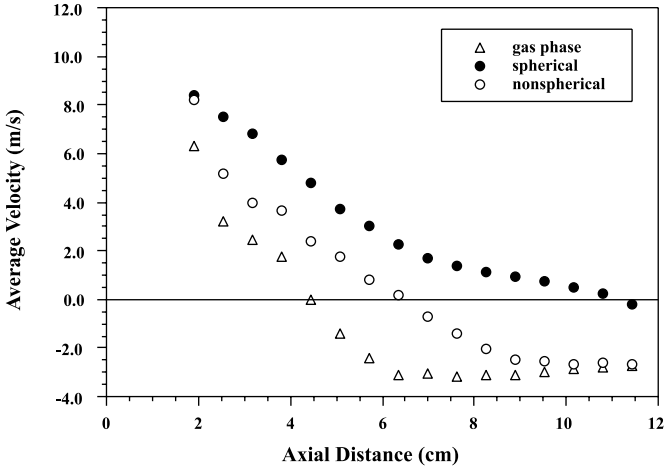

Fig. 10. Axial velocity profiles along the CFF centerline for the swirling flow case.

windows allowed a full traverse in one direction where the axial and tangential velocity components were determined. Only a partial traverse was possible in the orthogonal direction where the axial and radial velocity components are measured. However, the radial velocity is significant only in regions very near the inlet.

Figs. 10 and 11 show the axial profiles of average velocity in the axial direction (average velocities in the radial direction are zero at the centerline) and RMS velocities in the axial and radial directions along the vertical profile measured on the centerline near the top of the facility. In the swirling flow case the particle velocities decay more slowly than the gas phase due to the higher momentum of the larger particles as they enter the rapidly decelerating flow region below the primary air inlet. As shown in Fig. 10, the primary jet gas-phase velocity stagnates at a location just past the 4-cm location below the inlet. The corresponding particle stagnation points are located at 6.5 and 11 cm below the inlet for the nonspherical and spherical particles, respectively. It is interesting to note in Fig. 10 that the spherical particles penetrate the upper stagnation point in

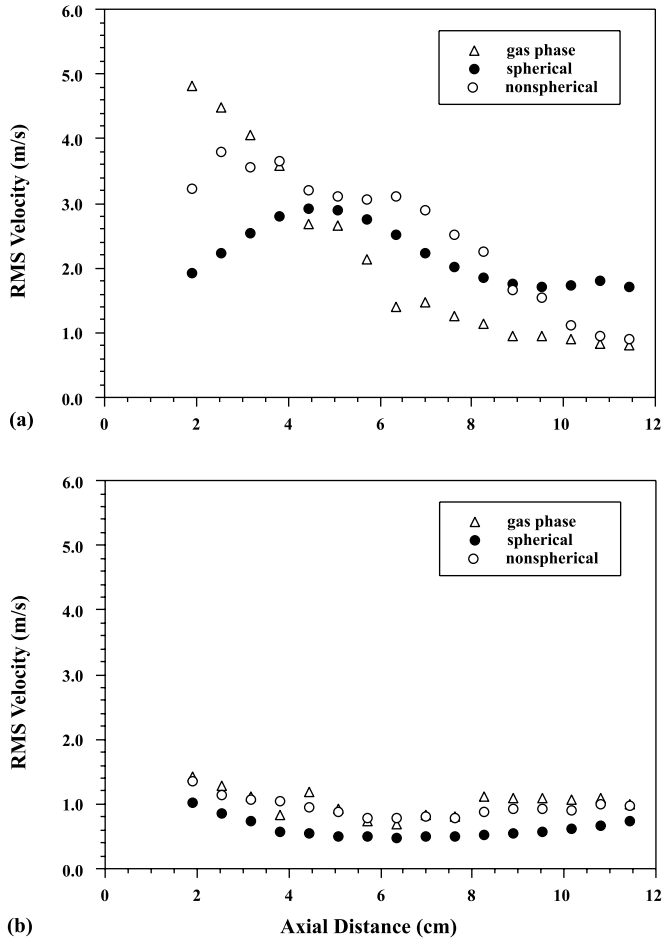

Fig. 11. RMS velocity profiles along the CFF centerline for the swirling flow case showing (a) the axial component and (b) the radial component.

the center of the flow chamber much further than the nonspherical particles as indicated by their significant positive velocity at locations further than 6.5 cm from the inlet. The velocity profile of the nonspherical particles falls in between the profiles measured for the spherical particles and the gas phase. This indicates that the nonspherical particles are able to better follow the gas velocity field, but that the momentum of the nonspherical particles still has a significant impact on their behavior.

The RMS velocity information shown in Fig. 11 illustrates that, for the most part, the RMS velocities for the nonspherical particles tend to fall somewhere between those measured for the spherical particles and the gas phases. In this region of the chamber, the axial RMS velocity values are significantly larger than the values measured in the radial direction. The trend in RMS velocity in the axial direction for the two particle types and the gas phase shows that the nonspherical particles start out at a velocity in between the spherical particles and the gas phase. It then decays in a similar fashion to the spherical particles but reaches a value close to that measured for the gas phase much more quickly than the spherical particles do. As discussed previously for the co-axial jet case, the RMS velocities tend to be high in regions of high velocity gradients. This effect is evident in Fig 17(a). The gas-phase mean axial velocity decays rapidly until reaching a value of about −3 m/s at a location 6 cm below the inlet. The gas-phase axial RMS velocity also changes rapidly until about this same axial location. For both the spherical and nonspherical particles, the axial RMS velocity is highest in the region where gradients are strongest. RMS velocities in the radial direction are very similar for both the gas phase and the nonspherical particles at about 1 m/s. Spherical particles have a slightly lower RMS velocity in that direction, averaging about 0.9 m/s over the profile.

According to work done by Haider and Levenspiel (1989) and Swamee and Ojha (1991), nonspherical particles tend to orient themselves to maximize the drag forces they are exposed to. Since the drag forces on the particles are one of the most significant factors affecting the particle dispersion, nonspherical particles may be able to follow the gas phase better if the orientation of the particle can respond quickly to the turbulent fluctuations. The particle response time (Lee et al., 1989) shows that increases in the drag coefficient for a given size particle would tend to decrease the particle time constant. This would indicate that the particles would be able to respond more rapidly to the turbulent fluctuations, behaving more closely to the gas phase. For example, a 30% increase in the drag coefficient, reported by Comer and Kleinstreuer (1995) for some spheriods, would cause the particle time constant to be reduced by about 23%. Also, the drag forces on nonspherical bodies are not necessarily parallel to the direction of motion (Clift et al., 1978). This could also increase the dispersion rates associated with nonspherical particles, causing them to behave more like the gas phase. Body forces (namely gravity) do not seem to be a significant factor in the data collected in the high-velocity region near the inlet.

In addition to identifying the centerline gas-phase stagnation point, as shown in Fig. 10, the stagnation point along the wall separating the upper and lower recirculation zones was also determined to more completely characterize the flow. Fig. 12 shows the axial velocity for the spherical particles and the gas phase measured 0.6 cm from the wall in the upper part of the flow chamber. No nonspherical particle data were taken at this location, since the purpose of the profiles shown was to determine the gas-phase information. The stagnation point identified in this profile along the wall is located approximately 12 cm below the inlet for both the gas phase and the spherical particles. This shows that at the swirl number selected for the operating condition,

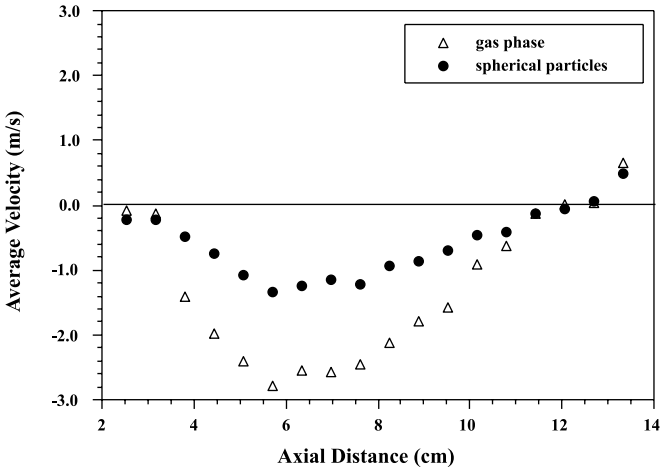

Fig. 12. Axial velocity profiles near the CFF wall for the swirling flow case showing the location of the stagnation point separating the outer and inner recirculation zones.

the upper recirculation zone is located only in a relatively small region in the top of the tube. Increasing the swirl number causes the size of this recirculation zone to decrease until it almost collapses against the top of the inlet. As expected, the gas-phase velocity exhibits much more variability than do the particles, as the flow first accelerates up the wall and then decelerates as it approaches the top of the chamber and turns back toward the centerline.

Figs. 13–16 show the radial mean and RMS velocity profiles measured for the swirling flow case in the upper two measurement locations. Data in these figures are plotted as radial profiles of axial, radial, and tangential velocity information (both mean and RMS) at the specified distance below the inlet in parts (a), (b), and (c), respectively. The mean velocity information for the location 2.5 cm below the inlet is shown in Fig. 13. In these results it is again evident that the average velocities for the nonspherical particles and gas phase are essentially the same. In the centerline under the primary jet, the flow is strongly decelerated to the upper stagnation point, where the gas flow is moving up the tube in the centerline. The larger spherical particles, with the higher momentum, decelerate less rapidly and therefore have higher mean velocities than the gas phase in this region of the flow. In the region under the swirling secondary air stream (located between 1 and 6 cm) the particle velocity is much lower than the gas-phase velocity as the particles present here are dispersing in from the primary jet or have been recirculated into the region via the upper recirculation zone. In the radial direction the axial velocity decreases rapidly, becoming negative for a short time, before increasing again and then finally decreasing toward the wall. This shows the center recirculation zone being established by the swirling flow just outside of the primary tube jet, as the velocities are negative for a short time for both the gas phase and the nonspherical particles. Spherical particles respond more slowly than the rapidly changing gas-phase velocity and do not have as large a region of negative velocity as does the gas phase and the nonspherical particles. The high velocity region centered at approximately 4 cm from the centerline corresponds to the region under the secondary jet as the flow from this part of the inlet moves outward and downward toward the wall.

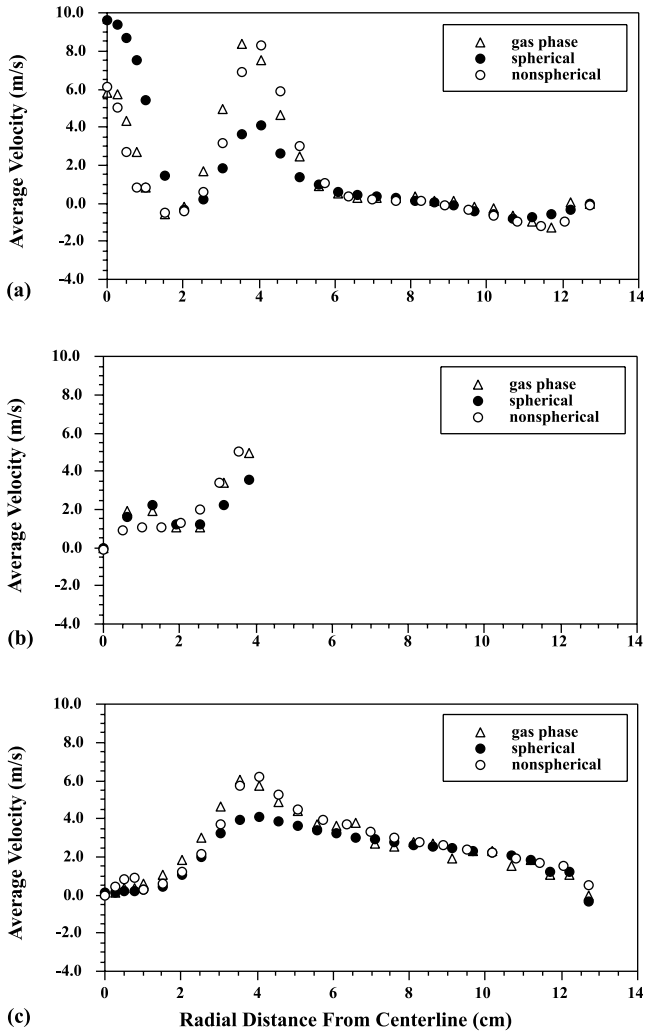

Fig. 13. Velocity profiles 2.5 cm below the inlet showing (a) axial, (b) radial, and (c) tangential velocity components in a swirling flow.

Profiles of radial velocity shown in Fig. 13(b) demonstrate the fairly significant mean radial velocities as the swirling flow responds to the sudden expansion in the area after the inlet to establishes the upper and lower recirculation zones. The average tangential velocity profiles in Fig. 13(c) show that this velocity component starts from zero at the centerline and increases rapidly to a location about 4 cm from the centerline, after which it decays gradually toward a zero value at the wall. The 4-cm radial location corresponds to a location just below the outside edge of the inlet where the highest tangential velocities in the inlet are seen.

The RMS velocity information for the three velocity components 2.5 cm below the inlet, shown in Fig. 14, again demonstrates the similarity of the nonspherical particle results to the gas-phase results. Overall the similarity between the nonspherical and spherical particle results as compared

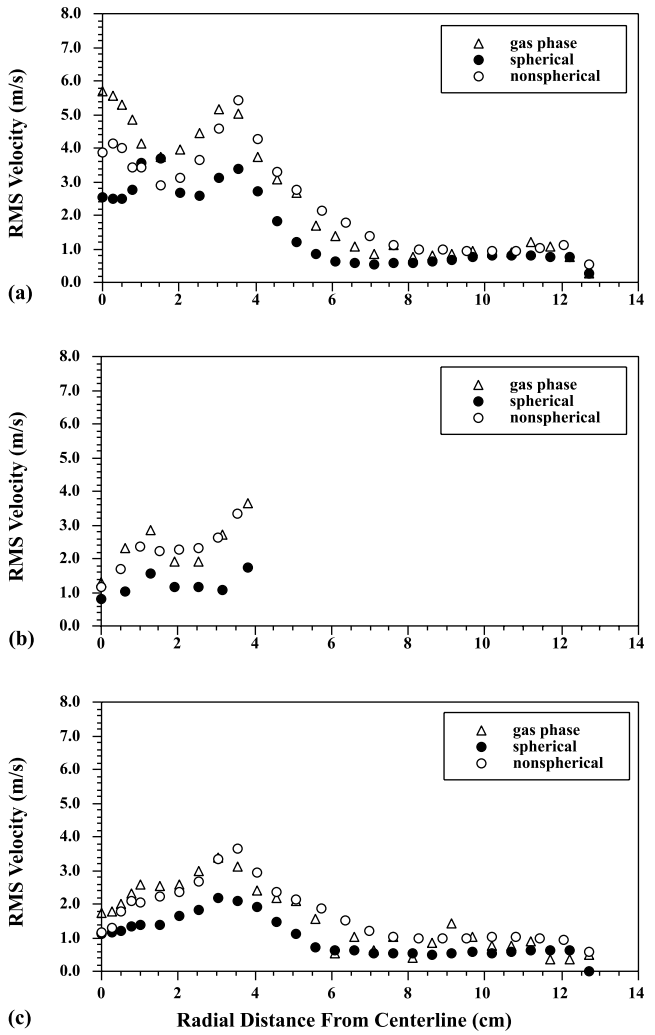

Fig. 14. RMS velocity profiles 2.5 cm below the inlet showing (a) axial, (b) radial, and (c) tangential components in a swirling flow.

to the gas phase are essentially the same except in the region near the centerline immediately under the primary jet where the particles enter the flow chamber. In this region the RMS velocity in the axial direction for the nonspherical particles falls midway between that measured for the gas phase and the spherical particles (Fig. 14(a)). This is caused by the significant influence of the particle momentum on their behavior making them less sensitive to the fluctuating gas-phase velocity, and therefore lowering their velocity. Due to the higher overall magnitude of the mean axial velocity, the RMS values associated with this component (shown in Fig. 14(a)) are considerably higher in this region of the flow facility than in the other two directions for all three components. RMS values for the gas phase show significant variations over the profile ranging from about 0.4 to 3 m/s. Overall the variation in the RMS values between the velocity components

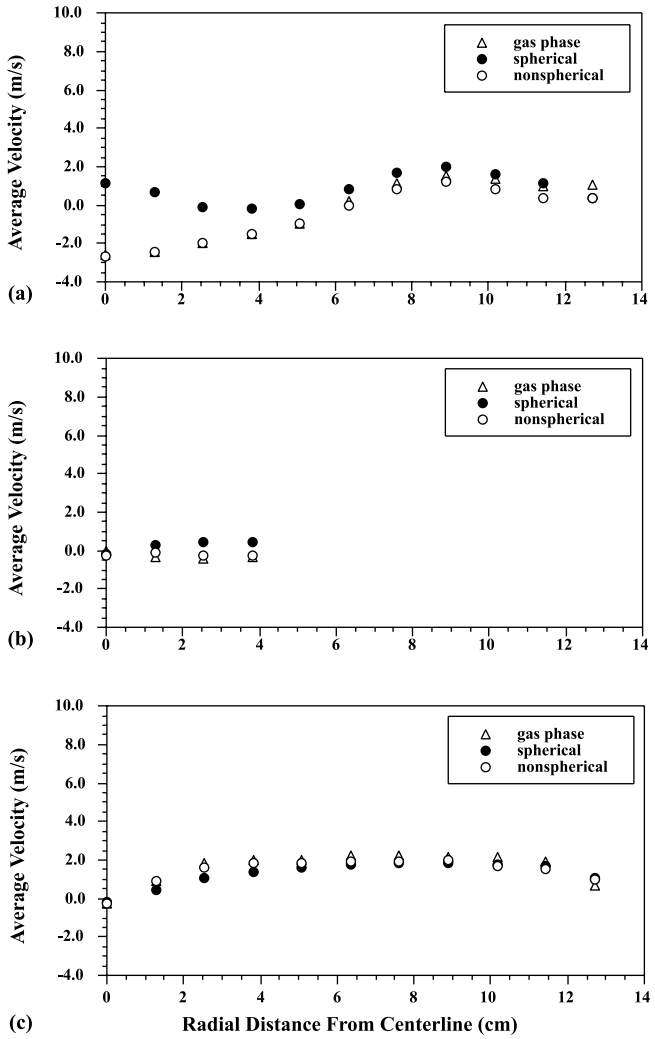

Fig. 15. Velocity profiles 10.8 cm below the inlet showing (a) axial, (b) radial, and (c) tangential velocity components in a swirling flow.

shown in Fig. 14 indicates that the turbulence in this region of the facility is nonisotropic for both the gas and particle flow fields.

As shown by the changes in the profiles between the location 2.5 cm below the inlet and the results of particle velocity and RMS velocity shown in Figs. 15 and 16 at a location 10.8 cm below the inlet, the velocity profiles change very quickly in swirling flows. This is in contrast to the information shown in the previous section for the co-axial jet case where fairly little decay of the velocity profiles occurred over the distance of 2.5–25.4 cm. The strong gradients present in the velocity profiles at 2.5 cm below the inlet (Fig. 13) have decreased greatly by the time the flow reaches the location 10.8 cm below the inlet. Measured velocities in the radial and tangential directions are beginning to reach the same values for all types of particles measured. The radial

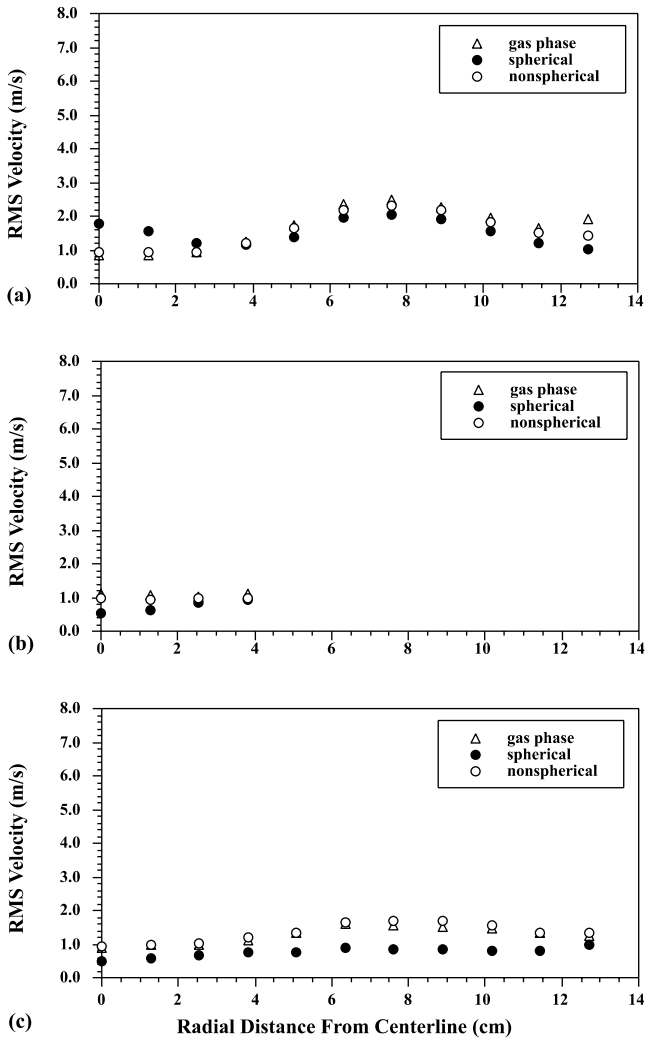

Fig. 16. RMS velocity profiles 10.8 cm below the inlet showing (a) axial, (b) radial, and (c) tangential components in a swirling flow.

velocities are slightly negative for both the gas phase and the nonspherical particles, while the spherical particles are still moving in the positive direction out toward the wall. A negative gas-phase velocity at this location is consistent with the flow structure typical of recirculating swirling flows. The profiles shown in Fig. 15 are measured in a region where the flow is turning back toward the centerline, giving the gas phase a slight negative velocity. The tangential velocity increases gradually from zero at the centerline to around 2 m/s when it then decays toward a zero value at the wall. Significant differences in the velocities between the particle types are still evident in the axial velocity results at this location. The spherical particle velocity at this point is still positive (or downward) while the nonspherical particles are moving in the negative direction (upward) with the gas phase. The two peaks in the spherical particle axial average velocity

(Fig. 15(a)) indicate that some of the largest particles coming from the inlet are still present in the centerline due to their high momentum while at the same time some of the particles have been entrained into the high velocity secondary jet that is moving toward the wall. This illustrates the significant variation in the flow structure between the different particle types in the upper region of the CFF. The spherical particles at the 10.8-cm location have a flow structure similar to that seen for the gas phase and the nonspherical particles at the 2.54-cm location (shown in Fig 13(a)) with a downward moving central jet of particles surrounded by a reverse flow region associated with the lower recirculation zone.

The RMS velocities at 10.8 cm below the inlet, shown in Fig 16, are continuing to decay and approach a common value in all direction as compared to those shown in Fig 14 at 2.5 cm below the inlet. For the gas phase and the nonspherical particles, RMS values in the radial direction are approximately constant at 1 m/s. In the tangential direction the RMS value varies from 1 to about 1.5 m/s. In both of these directions, the RMS velocity for the spherical particles is less than or about the same as those measured for the gas phase and the nonspherical particles. RMS values in the axial direction, shown in Fig. 16(a), range from about 1 to a little more than 2 m/s. The spherical particles demonstrate a larger spread in the results as the RMS value for this particle type at the centerline is about 1.8 m/s. It then decays to about 1 m/s at 3 cm, increases again to almost 2 m/s at 8 cm, and finally decays toward the wall. This trend is consistent with the velocity distribution seen in Fig. 15(a). RMS values in the axial direction peak again at the centerline due to the presence of the downward moving particles in that region that produce relatively high velocity gradients as compared to the gas phase and nonspherical particles. These gradients then produce a correspondingly high RMS velocity for the spherical particles in the axial direction near the centerline. RMS profiles for the nonspherical particles and the gas phase start at 1 m/s at the centerline, increase to a little over 2 m/s at 8 cm, and then decay toward the wall.

For the velocity profiles measured at 25.4 cm below the inlet, there is no appreciable difference in the results between the three different particle types. As expected, gradients are smaller now than at locations higher in the flow chamber. Axial velocities vary in an almost linear fashion from about −1.8 m/s at the centerline to about 1.5 m/s at 12 cm from the centerline when it then decays rapidly to zero at the wall. The radial velocity is essentially zero and the tangential velocity increases from zero at the centerline to 2 m/s at a location 4 cm from the wall where it then remains fairly constant almost to the wall before falling rapidly to zero. The RMS velocities measured for the three components are all nearly flat over the cross-section of the facility with variations ranging between 0.8 and 1 m/s. The rapid change in the flow structure seen in the swirling flow case is in sharp contrast to the structure seen in the co-axial jet flow where significant gradients are still present at the 25.4-cm location. In the swirling flow used here, all of the steep gradients and changes in flow structure are located in a small region near the top of the flow facility. After 25.4 cm below the inlet, axial gradients in the flow variables are quite small.

Profiles of velocity measured at 142 cm have nearly the same shape as discussed in the previous paragraph for the measurements done at 25.4 cm (see Black, 1997, for the complete data set). As in the information measured at that location, all three types of particles produced nearly identical results. This is true for both the velocities and the RMS velocities. Overall the RMS values at the 142-cm location decayed to about 0.5 m/s from the 0.8 m/s seen at 25.4 cm below the inlet. The exception to this is seen in the RMS profile for the tangential velocity component where values of

approximately 0.8 m/s are still measured at the centerline. At this location in the flow, all the particles are now in equilibrium with the gas phase and there is very little change in the flow structure in either the axial or radial directions as compared to the data taken at the 25.4-cm location. Also the turbulence in the flow field is beginning to approach an isotropic state with the exception of the centerline region where RMS velocities in the axial direction are still significantly higher than in the radial direction.

5.4. Size-resolved velocity

Since high number densities in addition to high velocity gradients are present along the axial profile at the reactor centerline for the swirling flow case, significant differences in the behavior of different particle sizes can occur. Fig. 17 shows the percentage of particles in each of the five discrete size classes, or bins, used in the analysis. Particles were divided into bins of 10 μm, starting at 30 μm and ending at 80 μm. As illustrated in the figure, most of the particles were in the 40–70 μm range with 10% or less of the particles in the bins above and below that range. It is interesting in this figure to note the effect of the stagnation point in the flow on the distribution of particle sizes in the overall distribution. The particles in the 30–50 μm range respond first to the gas-phase stagnation point which is located about 4 cm below the inlet. Especially in the 40–50 μm size class a significant reduction in the number of particles in this size range is seen after about 6 cm below the inlet. Particles in the 50–60 μm size range respond at a distance about 8 cm below the inlet. As the number of particles in the smaller size classes falls, the percentage in the larger sizes increases until that size responds to the reversed gas-phase flow field. Particles in the 60–70 μm size range do not respond to the stagnation point until they reach an axial location of about 11 cm below the inlet.

The average velocity information shown in Fig. 18 also demonstrates the ability of the particles to follow the gas phase. In the initial region close to the inlet, none of the larger particles are able to follow the gas phase. However the smaller particles are responding more quickly and do reach the gas phase values at a location 11 cm below the inlet. The larger the particle, the more

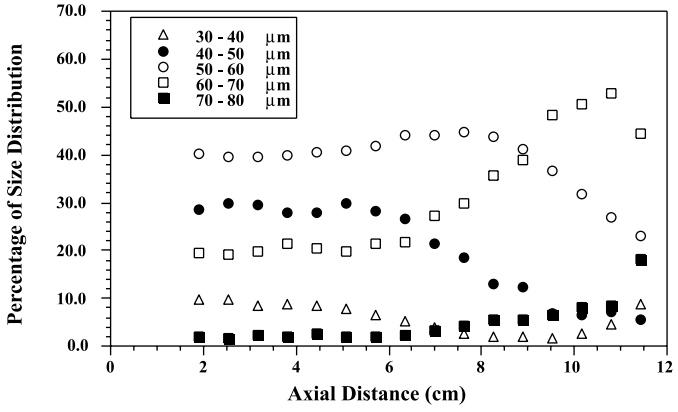

Fig. 17. Axial profiles of the percentage of spherical particles associated with different size classes within the overall distribution.

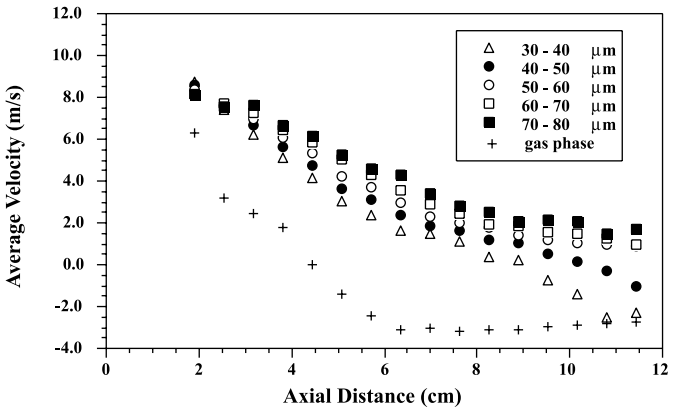

Fig. 18. Axial profiles of average velocity in the axial direction for the gas phase and spherical particles associated with different size classes within the overall distribution.

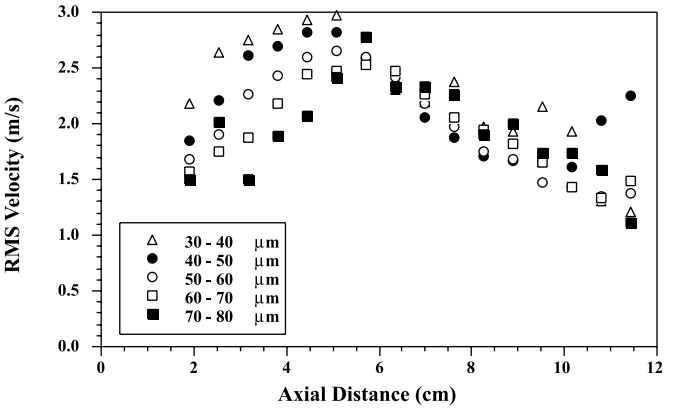

Fig. 19. Axial profiles of RMS velocity in the axial direction for spherical particles associated with different size classes within the overall distribution.

significant its momentum, and the slower the velocity of that size class decays. In the information shown, only the particles less than 50 μm are able to follow the gas phase in the lower recirculation zone and come back up the centerline. The large particles with the positive velocities are coming from the inlet and do no get recirculated by the flow field. Data for the axial component of RMS velocities, shown in Fig. 19, show that before the impact of the gas-phase stagnation point on the particle behavior, the smallest particles have the highest RMS velocities while the largest particles have the lower RMS due to the inertia and momentum effects of the particles as previously discussed. After the 6-cm location, no real strong trends in the data are evident. The increased spread in the data at the last axial locations is probably due to the decreased number of particles available for the analysis that tends to make the comparisons less accurate. For the radial component of RMS velocity, no real differences in the RMS values are seen for the different particle sizes used in this study. Values of 1.0 m/s were measured near the centerline, decaying to

0.5 m/s near the wall. This corresponds to the data shown in Fig. 11(b), where only a small difference between the gas phase and the spherical particle RMS velocity were seen.

6. Conclusions

A comprehensive data set of particle dynamics was collected on both a co-axial jet and a swirling flow. The data show that particle shape can have an important influence on the particle characteristics, especially when velocity gradients are high. The information also presents a detailed three-dimensional characterization of an idealized flow field that can be used for particle model validation. Data presented include profiles of mean velocity, RMS velocity, and size-resolved velocity.

Velocity profiles for both the co-axial jet and the swirling flow cases showed that significant differences in the profiles occur due to particle shape. This is especially true in the upper section of the flow chamber. In regions where the velocity gradients were high, the nonspherical particle velocity and RMS quantities tend to correspond very closely to the values measured for the gas phase. At other locations, little or no differences in the velocity profiles were observed. This is true except for the region immediately underneath the primary jet. Here the momentum of the nonspherical particles play a significant role, in addition to the drag characteristics, to cause the nonspherical velocity and RMS velocity to fall between the values determined for the gas phase and the spherical particles.

There are three principal reasons for the nonspherical particles to behave more closely to the gas phase than the spherical particles. First, the increase in the drag coefficient of nonspherical particles would tend to decrease the response time of the nonspherical particle, enabling them to respond faster to the turbulent fluctuations. Also, the drag forces acting on the particles are not necessarily in the direction of motion, depending on the particle orientation. This would cause the nonspherical particles to behave more like the gas phase than the equivalent size spherical particles. Finally, the terminal velocity of the nonspherical particles is lower than for the spherical particles. This effect shows up in the velocity profiles measured at the exit for both the swirling and co-axial jet flow conditions.

References

Akashi, K., Watanabe, J., Kenichi, K. 1979. Development of new flow rectifier for shortening upstream straight pipe length of flowmeter. In: Tokyo Flow Symposium, IMEKO Paper 12b-5, Society of Instrumentation and Control, Tokyo, pp. 279–284.

Alexander, D.R., Wiles, K.J., Schaub, S.A.,Seeman, M.P. 1985. Effects of non-spherical drops on a phase Doppler system. In: Chigier, N., Stewart, G.W. (Eds.), Particle Sizing and Analysis, Proceedings of SPIE 573, pp. 67–72.

Bachalo, W.D., Houser, M.J., 1984. Phase/Doppler spray analyzer for simultaneous measurements of drop size and velocity distributions. Opt. Eng. 23, 583–590.

Bachalo, W.D., Rudoff, R.C., Breña De La Rosa, A., 1988. Mass flux measurements of a high number density spray system using the phase Doppler particle analyzer. AIAA Paper, 88–0236.

Beér, J.M., Chigier, N.A., 1972. Combustion Aerodynamics. Applied Science Publishers, London.

Black, D.L., 1997. Experimental measurements of particle dispersion with spherical and nonspherical particles. Ph.D. Dissertation, Brigham Young University, Provo, UT.

Black, D.L., Mcquay, M.Q., Bonin, M.P., 1996. Laser-based techniques for particle size measurement: a review of sizing methods and their industrial applications. Prog. Energy Combust. Sci. 22, 267–306.

Bonin, M.P., 1992. Optical measurements of particle size, velocity, and number density in two- phase, isothermal, and reacting flows. Ph.D. Dissertation, Brigham Young University, Provo, UT.

Breña De La Rosa, A., Sankar, S.V., Wang, G., Bachalo, W.D., 1993. Particle diagnostics and turbulence measurements in a confined isothermal liquid spray. J. Eng. Gas Turb. Power 115, 499–506.

Butler, B.W., Webb, B.W., 1993. Measurement of radiant heat flux and local particle and gas temperatures in a pulverized coal-fired utility scale boiler. Energy Fuels 7, 835–841.

Call, C.J., Kennedy, I.M., 1992. Measurements and simulations of particle dispersion in a turbulent flow. Int. J. Multiphase Flow 18, 891–903.

Clift, R., Grace, J.R., Weber, M.E., 1978. Bubbles, Drops, and Particles. Academic Press, New York.

Comer, J.K., Kleinstreuer, C., 1995. A numerical investigation of laminar flow past nonspherical solids and droplets. J. Fluids Eng. 117, 170–175.

Crowe, C.T., Troutt, T.R., Chung, J.N., 1996. Numerical models for two-phase turbulent flows. Annu. Rev. Fluid. Mech. 28, 11–43.

Edwards, C.F., Marx, K.D., 1992. Analysis of the ideal phase-Doppler system: limitations imposed by the single particle constraint. Atom. Sprays 2, 319–366.

Faeth, G.M., 1983. Recent advances in modelling particle transport properties and dispersion in turbulent flow. Proc. ASME–JSME Therm. Eng. Conf. 2, 517–534.

Frank, T.H., Schade, K.P., Petrak, D., 1993. Numerical simulation and experimental investigation of a gas-solid two-phase flow in a horizontal channel. Int. J. Multiphase Flow 19, 187–198.

Ganser, G.H., 1993. A rational approach to drag prediction of spherical and nonspherical particles. Powder Technol. 77, 143–152.

Gupta, A.K., Lilley, D.G., Syred, N., 1984. Swirl Flows. Abacus Press, Kent.

Haider, A., Levenspiel, O., 1989. Drag coefficient and terminal velocity of spherical and nonspherical particles. Powder Technol. 58, 63–70.

Hallett, W.L.H., 1986. Swirl generator for independent variation of swirl and velocity profile. AIAA J. 24, 1212–1213.

Hallett, W.L.H., Tavasoli, V., 1991. The effect of a central hub on critical swirl in a swirling sudden-expansion flow. J. Inst. Energy 64, 82–88.

Hallett, W.L.H., Toews, D.J., 1987. The effects of inlet conditions and expansion ratio on the onset of flow reversal in swirling flow in a sudden expansion. Exp. Fluids 5, 129–133.

Hartman, M., Trnka, O., Svoboda, K., 1994. Free settling of nonspherical particles. Ind. Eng. Chem. Res. 33, 1979–1983.

Hishida, K., Ando, A., Maeda, M., 1992. Experiments on particle dispersion in a turbulent mixing layer. Int. J. Multiphase Flow 13, 181–194.

Klett, J.D., 1995. Orientation model for particles in turbulence. J. Atmos. Sci. 52, 2276–2285.

Lamb, R.G., 1980. Mathematical principles of turbulent diffusion modelling. Developments in atmospheric science 11. In: Longhetto, A. (Ed.), Atmospheric Planetary Boundary Layer Physics. Elsevier, Amsterdam, pp. 173–210.

Lee, M.M., Hanratty, T.L., Adrian, R.J., 1989. An axial viewing photographic technique to study turbulence characteristics of particles. Int. J. Multiphase Flow 15, 787–802.

Liu, C.J., Nouri, J.M., Whitelaw, J.H., Tse, D.G.N., 1989. Particle velocities in a swirling, confined flow. Combust. Sci. Technol. 68, 131–145.

Mcdonell, V.G., Samuelsen, G.S., 1990. Application of laser interferometry to the study of droplet/gas phase interactions and behavior in liquid spray combustion systems. Combust. Sci. Technol. 74, 343–359.

Mcdonell, V.G., Samuelsen, G.S., 1992. Optical measurements of gas phase vector and scalar properties in reacting and non-reacting sprays. In: Durao, D.F.G., et al. (Ed.), Combusting Flow Diagnostics. Kluwer Academic Publishers, London, pp. 305–323.

Parthasarathy, R.N., Faeth, G.M., 1990. Turbulent dispersion of particles in self-generated homogeneous turbulence. J. Fluid Mech. 220, 515–537.

Phillips, S.D., 1989. Data book for evaluation of three-dimensional combustion models. M.S. Thesis, Brigham Young University, Provo, UT.

Shirolkar, J.S., 1996. Modeling turbulent particle dispersion in dilute, nonreacting flows. Ph.D. Dissertation, Brigham Young University, Provo, UT.

Shirolkar, J.S., Coimbra, C.F.M., Mcquay, M.Q., 1996. Fundamental aspects of modeling turbulent particle dispersion in dilute flows. Prog. Energy Combust. Sci. 22, 363–399.

Sommerfeld, M., 1990. Particle dispersion in turbulent flow: the effect of particle size distribution. Part. Part. Syst. Charact. 7, 209–220.

Sommerfeld, M., Ando, A., Wennerberg, D., 1992. Swirling, particle-laden flows through a pipe expansion. J. Fluids Eng. 114, 648–656.

Sommerfeld, M., Qiu, H.-H., 1991. Detailed measurements in a swirling particulate two-phase flow by a phase-Doppler anemometer. Int. J. Heat Fluid Flow 12, 20–28.

Sommerfeld, M., Qiu, H.-H., 1993. Characterization of particle-laden, confined swirling flows by phase-Doppler anemometry and numerical calculation. Int. J. Multiphase Flow 19, 1093–1127.

Swamee, P.K., Ojha, C.S.P., 1991. Drag coefficient and fall velocity of nonspherical particles. J. Hydraul. Eng. 117, 660–667.

Syred, N., Beér, J.M., 1974. Combustion in swirling flows: a review. Combust. Flame 23, 143–201.

Truelove, J.S., 1986. Prediction of the near-burner flow and combustion in swirling pulverized-coal flames. In: 21st Symposium (International) on Combustion, The Combustion Institute, Pittsburgh, PA, pp. 275–284.

Wang, L.-P., Stock, D.E., 1993. Dispersion of heavy particles by turbulent motion. J. Atmos. Sci. 50, 1897–1913.

Wang, H., Mcdonell, V.G., Sowa, W.A., Samuelson, S., 1994a. Experimental study of a model gas turbine combustor swirl cup: Part 1: two-phase characterization. J. Prop. Power 4, 441–445.

Wang, H., Mcdonell, V.G., Sowa, W.A., Samuelson, S., 1994b. Experimental study of a model gas turbine combustor swirl cup: Part2: droplet dynamics. J. Prop. Power 4, 446–452.